Secondary Breakup of Non-Newtonian Liquid Drops

C. López-Rivera* and P. E. Sojka
Maurice J. Zucrow Laboratories
Department of Mechanical Engineering
Purdue University
West Lafayette, IN 47907-2014 USA

Abstract

The secondary breakup of non-Newtonian liquid drops was investigated experimentally to determine breakup morphology and initial breakup time. Xanthan gum-water solutions with concentrations ranging from 0.05 to 0.25% by weight were formed into drops and injected into a high speed air stream. Drop morphology was captured using a high-speed (6688 fps) imaging system. Breakup times were determined from these images. Bag and multimode breakup regime boundaries for non-Newtonian drops were found to occur at Weber numbers close to those reported for Newtonian liquids. In contrast, sheet-thinning breakup was observed at Weber number values smaller than for Newtonian drops. In contrast to Newtonian results, significant bag growth and stretching was observed prior to breakup. In addition, after breakup not only were drops found, but also ligaments. As expected, an increase in Weber number lead to more violent breakup. Dimensionless initial breakup times were independent of Weber number and approximately 60% higher than those of Newtonian drops under the same conditions. Finally, increases in Ohnesorge number were observed to produce increases in initial breakup time. Based on data illustrating the effects of variations in liquid rheology on drop morphology and breakup times, we conclude that the behavior of even low concentration non-Newtonian liquids deviates from that reported for Newtonian liquids.

Introduction

The literature is rich in studies that describe the breakup (secondary atomization) of Newtonian liquid drops. Groups including [7, 8, 11, 12, 15-17] and others have investigated Newtonian drop secondary breakup and identified the mechanics of the processes. Their contributions describe the existence of several breakup modes for low Ohnesorge numbers (*Oh*), i.e. when liquid viscous effects are minimal. Each of these modes reveals qualitative differences in breakup mechanisms and produce different outcomes for fragment sizes. Various correlations have also been proposed for predicting the initial and total breakup times.

In contrast to the Newtonian case, very few studies have considered non-Newtonian drop breakup. These include [1, 2, 9, 10, 13, 14, 18], who have reported that secondary breakup differs from that of Newtonian liquids. However, there is still not enough data to provide a clear consensus as to either common characteristics or processes for non-Newtonian drop secondary breakup. Questions currently confronting the spray community include:

- "What is the morphology of non-Newtonian liquid drops undergoing secondary breakup?"
- Given the breakup modes for non-Newtonian liquid drops, "What are the Weber numbers (*We*) at the boundaries between the various modes? What is the *Oh* scaling of *We* at these boundaries? What are the initial and total drop breakup times?"

We have begun answering these questions by making experimental measurements of drop morphology, plus initial breakup times, using high speed digital imaging. The results are important since they will significantly impact fields such as mass spectrometry, pharmaceutical manufacturing, consumer products, gelled fuels for missile propulsion, food processing, and paints/coatings processes, all of which rely on non-Newtonian liquids and require accurate knowledge of drops sizes for their optimization.

Experimental Apparatus

Experiments were performed by using a drop generator to produce a stream of uniform size drops, and then injecting them into a horizontal gas jet formed using an air nozzle. The liquid flow was supplied by a syringe with the flow rate adjusted to achieve steady streams of drops having diameters between 1.9 and 2.6 ± 0.1 mm. See Fig. 1.

*lopez0@purdue.edu

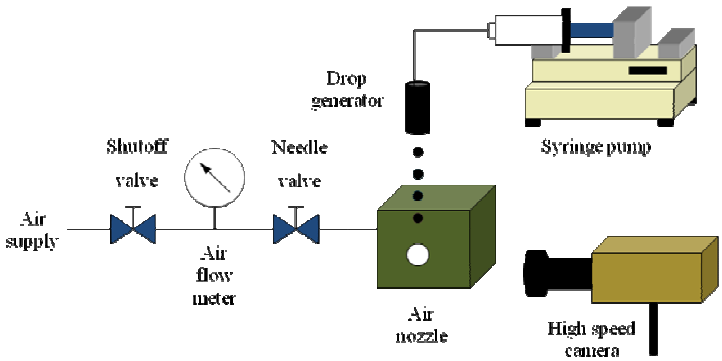

Figure 1. System schematic

Three solutions were formulated by dissolving Xanthan gum (XG) in water with concentrations ranging from 0.05 to 0.25% by weight. They can be treated as power-law fluids, so their rheology is described by (1), where τ is the shear stress, K the consistency index, γ the strain rate and n the flow behavior index:

$$\tau = K\dot{\gamma}^n \qquad (1)$$

Liquid rheology was measured using a TA Instruments AR-G2 rheometer. Power law indices for the solutions were determined by a fit to the shear stress versus strain rate data with r^2 greater than 0.997.

Liquid densities (ρ_{liq}) were measured by weighing a known volume on a Sartorius analytical balance. Surface tensions (σ_{liq}) were determined using a Cenco DuNuoy tensiometer. Data for all solutions are listed in Table 1.

Table 1. Physical properties of Xanthan Gum-water solutions.

Xanthan gum concentration (wt-%)	Flow behavior index, n	Consistency index, K (Pa-s)	Surface tension, σ_{liq} (N/m)	Density, ρ_{liq} (kg/m^3)
0.05	0.513	0.111	0.072 ± 0.001	999 ± 1.0
0.10	0.413	0.311	0.072 ± 0.001	999 ± 1.0
0.25	0.313	1.024	0.073 ± 0.001	999 ± 1.0

The air nozzle generated a jet with a nearly-uniform velocity profile. LDA and PIV axial velocity measurements through the nozzle centerline at various locations showed the uncertainty is ± 3% of the mean.

Time dependent drop behavior was recorded using a Vision Research Phantom v7.3 high speed digital camera mated to a Nikon lens with a focal length of 105 mm. Images of 800×600 pixels were recorded at 6688 fps. A Kratos 1000 W Xe arc lamp was used as an illumination source. It produced a collimated beam, which reflected off a dichroic mirror that filtered out the IR and UV components, after which a plano-convex lens focused it onto an opal glass diffuser. The diffuser scattered the collimated beam and backlit the drop breakup process. See Fig. 2.

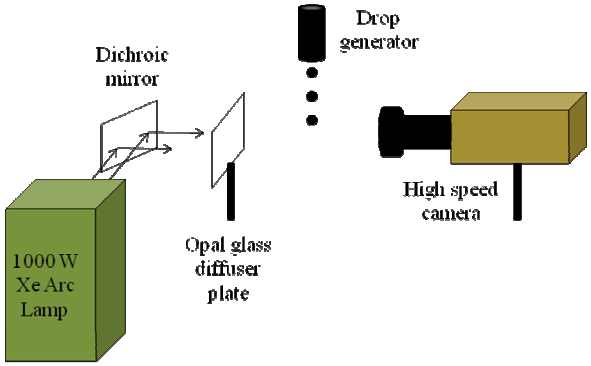

Figure 2. High speed imaging system

A calibration key was created as part of the optical system. It enabled direct measurement of drop diameter and determination of the axial and radial locations with respect to the air nozzle exit. It also facilitated determination of the air velocity at drop breakup since LDA results were mapped onto the recorded images.

Results and Discussion

In this investigation, drop behavior was analyzed in terms of *We*, *Oh* and the dimensionless breakup time (*T*). These are given by (2), (3) and (4), respectively. In these expressions, ρ_{air} is the air density, V_0 is the initial relative velocity between the drop and the surrounding air, D_0 is the initial drop diameter and *t* is the time:

$$We = \frac{\rho_{air} V_0^2 D_0}{\sigma_{liq}} \qquad (2)$$

$$Oh = \frac{K}{D_0^{n-1/2} V_0^{1-n} \sqrt{\rho_{liq} \sigma_{liq}}} \qquad (3)$$

$$T = t \frac{V_0}{D_0} \sqrt{\frac{\rho_{air}}{\rho_{liq}}} \qquad (4)$$

The experimental system can provide *We* and *Oh* values up to 60 and 0.0056, respectively. Since the experiments have three independently controllable parameters: drop diameter, relative velocity and droplet viscosity, *We* and *Oh* values can be specified independently.

Breakup morphology

Non-Newtonian drop breakup morphology was found to depend on *We* and *Oh*. For instance, Fig. 3 shows typical bag breakup (top row) for the 0.05% XG solution. This regime was observed to start at *We*~12 and *Oh*~0.0035, *We*~12 and *Oh*~0.0040, and *We*~13 and *Oh*~0.0054 for the 0.05, 0.10, and 0.25% XG solutions, respectively. These values are similar to those reported by [3] for Newtonian liquids (*We*=13 for *Oh*<0.1).

Figure 4 contains *We* values at bag breakup onset for all solutions studied. The data is compared to Brodkey's correlation for critical Weber number (We_c), reported by [15], and to those predicted by [5]. As can be observed, the experimental values with the highest *Oh* for each of the solutions are located in the vicinity of those predicted for Newtonian drops. This confirms that drop breakup starts at *We* and *Oh* values similar to those for Newtonian drops. Also, increases in *Oh* lead to increases in *We*, as expected, due to the rheological nature of the solutions.

The onset of the multimode breakup regime (also known as bag-and-stamen breakup) was observed when *We* and *Oh* were increased to ~16 and ~0.0032, ~18 and ~0.0036, and ~19 and ~0.0048 for the 0.05, 0.10, and 0.25% XG solutions, respectively. These results are also similar to the Newtonian ones reported by [3], for which the multimode breakup regime was observed to begin at a *We*=18 for *Oh*<0.1. Fig. 3 (middle row) shows a typical multimode breakup for the 0.05% XG solution.

The similarities between the Newtonian and non-Newtonian bag and multimode breakup modes are ascribed to the low concentration values of the solutions under study. It is probable that higher polymer concentrations could cause the breakup process to deviate from that of Newtonian drops. This will be addressed in a future study.

Regardless of similarities, notable differences between the Newtonian and non-Newtonian cases are the significant growth and stretching of the non-Newtonian bags before break up and the appearance of protrusions at the edges of their rims, which elongate upstream. This is shown in Fig. 3 for *T*=3.06. As expected, increases in polymer concentration led to more significant bag growth and stretching. This is attributed to liquid rheology (higher *K* values) producing stronger consolidating forces. Finally, it can also be observed that the bag breaks into both ligaments and drops, and not directly into drops as occurs in Newtonian cases.

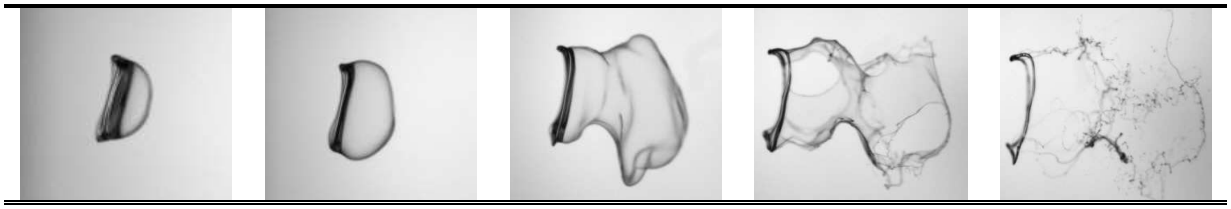

T=2.50 *T*=2.71 *T*=3.06 *T*=3.27 *T*=3.41

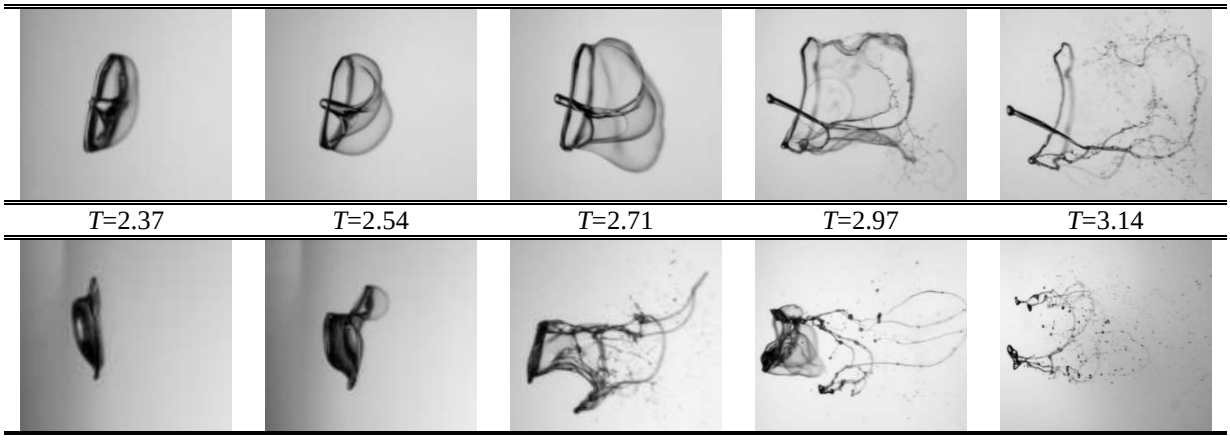

Figure 3. Typical bag, multimode and sheet-thinning breakup events (0.05% XG solution)

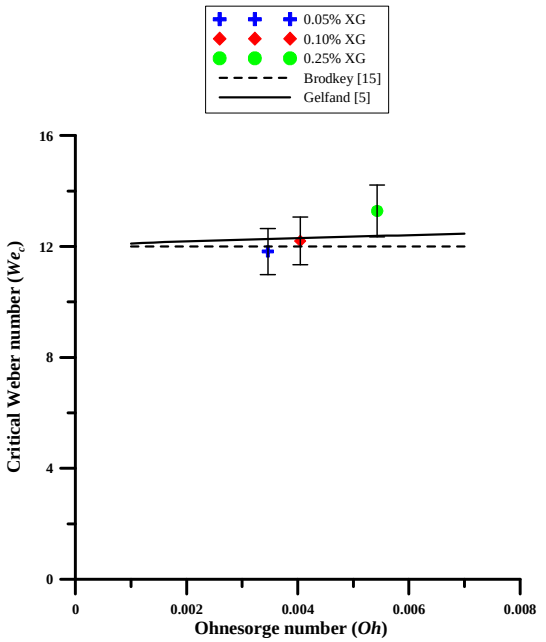

Figure 4. Critical Weber number (We_c) versus Ohnesorge number (Oh)

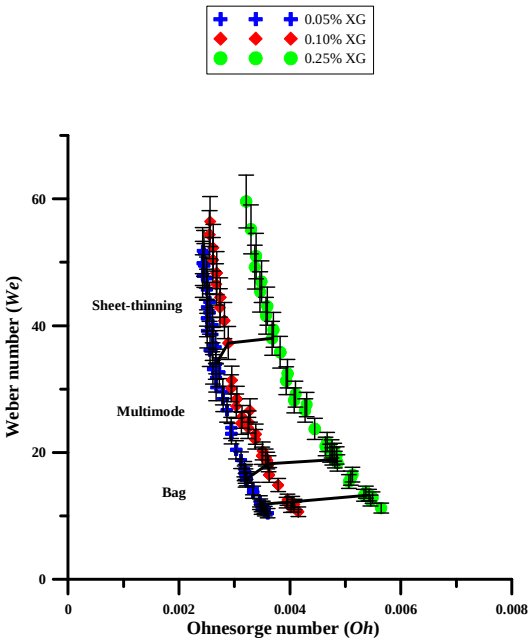

Figure 5. Weber number (*We*) versus Ohnesorge number (Oh)

The sheet-thinning breakup regime (also known as shear stripping) was observed when *We* and *Oh* were increased to ~34 and ~0.0027, ~37 and ~0.0029, and ~38 and ~0.0037 for the 0.05, 0.10, and 0.25% XG solutions, respectively. Contrary to the results for the other breakup modes, these differ significantly from their Newtonian counterparts, as reported by [3], for which the regime was observed to begin at a *We*=80 for *Oh*<0.1. Fig. 3 (bottom row) shows a typical sheet-thinning breakup for the 0.05% XG solution. In addition, this figure shows some remarkable differences in the breakup process. Here, bags are formed from the liquid sheet that is being peeled off at the edges of the core, instead of a stripping process generating drops. After these bags burst, the core starts to disrupt forming bags, drops and eventually a cloud of ligaments and drops, as reported by [1, 2, 9 and 18]. The differences are ascribed to the complex rheology that these solutions exhibit.

Figure 5 is a breakup regime boundary plot. Similar to the Newtonian case, regime boundaries do not depend on *Oh*. This is attributed to the low concentration values of the solutions studied. The behavior could deviate significantly from that of Newtonian drops for higher concentrations. This will also be addressed in a future study.

Breakup times

Two times are frequently encountered in the literature: the initial and the total breakup times. The initial breakup time is the interval between when the drop is injected into the air jet and the point where it deforms into an oblate ellipsoid shape. The total breakup time is defined as the time when no further breakup occurs. Both are commonly reported in their non-dimensional form, as given by (4).

Fig. 6 illustrates the dependence of the dimensionless initial breakup time (T_{ini}) on *We*. Note the unexpected independence of T_{ini} on *We*. Also note that T_{ini} values for the three solutions are similar. This could be due to the fact that their polymer concentrations do not span a wide enough range to cause significant differences.

Regardless, these results are not qualitatively consistent with the Newtonian correlation reported by [15], which has been plotted for the minimum and maximum *Oh* values (0.0024 and 0.0056) obtained in this study. The experimental values are approximately 60% higher than the predicted values. This occurs because the non-Newtonian solutions have higher effective viscosity values (higher *K*), which retards their breakup.

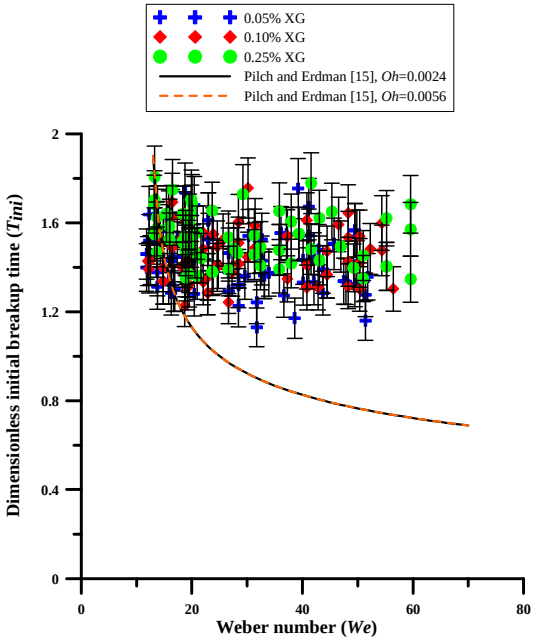

Figure 6. Dimensionless initial breakup time **(**T_{ini}) versus Weber number (*We*)

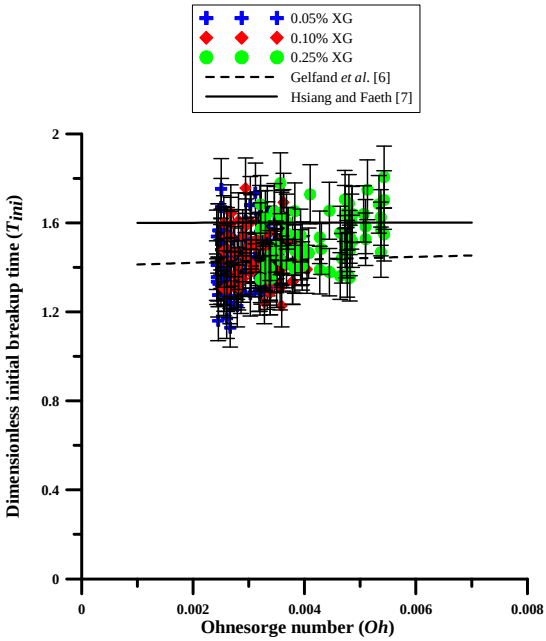

Figure 7. Dimensionless initial breakup time **(**T_{ini}) versus Ohnesorge number (*Oh*)

The relationship between T_{ini} and *Oh* is shown in Fig. 7. As expected, an increase in *Oh* leads to an increase in T_{ini} for all solutions, since increases in *Oh* result from increasing *K* and consequently the consolidating forces retarding the drop breakup process. One surprising finding was that similar T_{ini} values were obtained for all three solutions. This is also ascribed to the small span in their polymer concentrations. In addition, good agreement was observed between experimental results and the correlations of [6] and [7], with all points lying within 25% of these Newtonian correlations. Note that the [6] correlation provides a better qualitative match to the data.

Finally, it was not possible to capture the dependence of the dimensionless total breakup time (T_{tot}) on *We* since ligaments formed as a result of breakup tend to travel further distances downstream before fragmenting than our current experimental setup can capture. Because of this, further studies capable of capturing the complete breakup process are required.

Summary and Conclusions

The breakup behavior of non-Newtonian liquid drops was recorded for a variety of *We* and *Oh* values. Three regimes were observed: bag, multimode and sheet-thinning. *We* and *Oh* values that demark boundaries between these regimes were reported. *We* values for the bag and multimode regimes were found to be similar to those reported for Newtonian liquids, while *We* for the sheet-thinning differs significantly. Key features of these regimes were the larger growth of the bags and the formation of ligaments, as compared to those for Newtonian drops.

T_{ini} data were also presented. Unexpectedly, T_{ini} was independent of *We* and increases with increases in *Oh*. Also, T_{ini} values were found to be similar to those predicted by correlations [6-7] developed for Newtonian drops to within experimental uncertainties.

Nomenclature

D initial drop diameter
K consistency index
n flow behavior index
Oh Ohnesorge number
t time
T dimensionless breakup time
V initial relative velocity between the drop and the surrounding air
We Weber number
γ strain rate
ρ density
σ surface tension
τ shear stress

Subscripts
air air
c critical
ini initial
liq liquid
tot total

References

1. Arcoumanis, C., Khezzar, L., Whitelaw, D.S., and Warren, B.C.H., *Experiments in Fluids*, 17:405-414 (1994).
2. Arcoumanis, C., Whitelaw, D.S., and Whitelaw, J.H., *Atomization and Sprays*, 6:245-256 (1996).
3. Dai, Z., and Faeth, G.M., *International Journal of Multiphase Flow*, 27:217-236 (2001).
4. Fox, R.W., and McDonald, A.T., *Introduction to Fluid Mechanics*, John Wiley & Sons, Inc., 1998, p. 732-737.
5. Gelfand, B.E., *Progress in Energy Combustion Science*, 22:201-265 (1996).
6. Gelfand, B.E., Gubin, S.A., Kogarko, S.M., and Komar, S.P., *Journal of Engineering Physics and Thermophysics*, 25:1140-1142 (1973).
7. Hsiang, L.-P., and Faeth, G.M., *International Journal of Multiphase Flow*, 18:635-652 (1992).
8. Hsiang, L.-P., and Faeth, G.M., *International Journal of Multiphase Flow*, 21:545-560 (1995).
9. Joseph, D.D., Beavers, G.S., and Funada, T., *Journal of Fluid Mechanics*, 453:109-132 (2002).
10. Joseph, D.D., Belanger, J., and Beavers, G.S., *International Journal of Multiphase Flow*, 25:1263-1303 (1999).
11. Krzeczkowski, S.A., *International Journal of Multiphase Flow*, 6:227-239 (1980).
12. Liu, Z., and Reitz, R.D., *International Journal of Multiphase Flow*, 23:631-650 (1997).
13. Matta, J.E., and Tytus, R.P., *Journal of Applied Polymer Science*, 27:397-405 (1982).
14. Matta, J.E., Tytus, R.P., and Harris, J.L., *Chemical Engineering Communications*, 19:191-204 (1983).
15. Pilch, M., and Erdman, C.A., *International Journal of Multiphase Flow*, 13:741-757 (1987).
16. Ranger, A.A., and Nicholls, J.A., *American Institute of Aeronautics and Astronautics Journal*, 7:285-290 (1969).
17. Wierzba, A., and Takayama, K., *American Institute of Aeronautics and Astronautics Journal*, 26:1329-1335 (1988).
18. Wilcox, J.D., June, R.K., Brown, H.A., and Kelly, R.C., *Journal of Applied Polymer Science*, 5:1-6 (1961).